JOURNAL OF PETROLOGY | VOLUME 43 | NUMBER 7 | PAGES 1311–1326 | 2002

Volatiles in Submarine Basaltic Glasses from the Northern Kerguelen Plateau (ODP Site 1140): Implications for Source Region Compositions, Magmatic Processes, and Plateau Subsidence

PAUL J. WALLACE*

OCEAN DRILLING PROGRAM, TEXAS A&M UNIVERSITY, COLLEGE STATION, TX 77845, USA

RECEIVED JUNE 29, 2001; REVISED TYPESCRIPT ACCEPTED FEBRUARY 1, 2002

Submarine pillow basalts (34 Ma) recovered from the Northern Kerguelen Plateau at ODP Site 1140 contain abundant unaltered glass, providing the first opportunity to measure the volatile contents of tholeiitic basaltic magmas related to the Kerguelen mantle plume. The glasses have La/Sm and Nb/Zr ratios that vary from values similar to Southeast Indian Ridge (SEIR) MORB (Unit 1), to slightly more enriched (Unit 6), to values transitional between SEIR MORB and basaltic magmas formed by melting of the Kerguelen plume (Units 2 and 3). Volatile contents for glasses in Units 1 and 6 are similar to depleted mid-ocean ridge basalt (MORB) values (0·25–0·27 wt % H_2O, 1240–1450 ppm S, 42–54 ppm Cl). In contrast, H_2O contents are higher for the enriched glasses (Unit 2, 0·44 wt % H_2O; Unit 3, 0·69 wt %), as are S (1500 ppm) and Cl (146–206 ppm). Cl/K ratios for all glasses are relatively low (0·03–0·04), indicating that assimilation of hydrothermally altered material did not occur during shallow-level crystallization. H_2O/Ce for the enriched glasses (Units 2 and 3) is significantly lower than Pacific and South Atlantic MORB values, suggesting that low H_2O/Ce may be an inherent characteristic of the Kerguelen plume source. Vapor saturation pressures calculated using the H_2O and CO_2 contents of the glasses indicate that ~1700 m of subsidence has occurred on this part of the plateau since eruption of the basalts at 34 Ma. Subsidence estimates for Site 1140 and other ODP drill sites indicate that the various parts of the Kerguelen Plateau subsided at a rate comparable with that for normal Indian Ocean lithosphere.

KEY WORDS: *basaltic glass; Kerguelen plume; trace elements; volatiles; water*

INTRODUCTION

The Kerguelen Plateau and Broken Ridge formed mostly during the Cretaceous as a single, giant oceanic plateau that is interpreted to represent voluminous magmatism associated with emplacement of a mantle plume head below young Indian Ocean lithosphere (Duncan & Storey, 1992; Weis *et al.*, 1992). During Ocean Drilling Program (ODP) Leg 183, igneous basement rock and sediment cores were obtained from five sites on the Kerguelen Plateau and two on Broken Ridge (Fig. 1). The results, combined with subsequent radiometric dating, demonstrate that from south to north the age of the uppermost crust decreases from 120–110 Ma in the Southern Kerguelen Plateau, to ~110 to 95 Ma in the Central Kerguelen Plateau, Broken Ridge and Elan Bank, to ≤35 Ma in the Northern Kerguelen Plateau (Coffin *et al.*, 2000; Pringle & Duncan, 2000; Duncan, 2002). At six of seven basement sites, as well as at four sites drilled on earlier ODP cruises, subaerially erupted basalt flows were recovered, indicating that the growth rate of the Kerguelen large igneous province (LIP) was sufficient to form a subaerial landmass. However, a sequence of submarine-erupted pillow basalt flows of 90 m thickness was drilled at Site 1140 on the Northern Kerguelen Plateau (Coffin *et al.*, 2000).

The Site 1140 submarine glasses provide the first opportunity to measure the volatile contents of tholeiitic basaltic magmas related to the Kerguelen mantle plume.

*Present address: Department of Geological Sciences, University of Oregon, Eugene, OR 97403-1272, USA. Telephone: (541) 346-5985. Fax: (541) 346-4692. E-mail: pwallace@darkwing.uoregon.edu

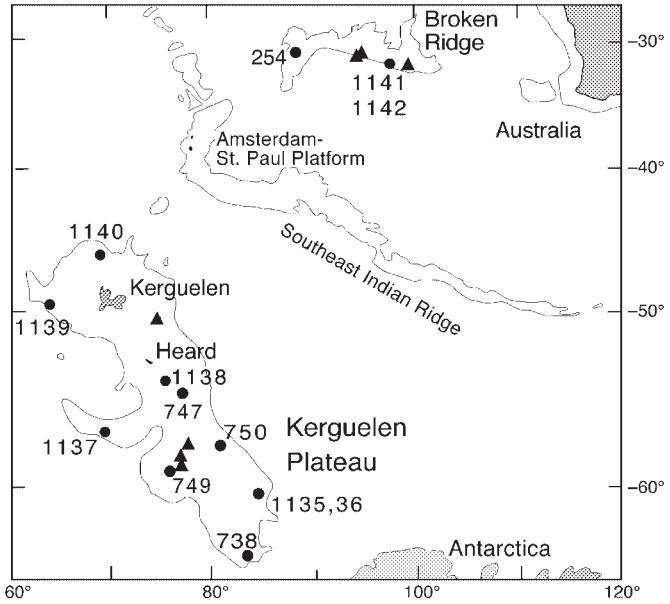

Fig. 1. Location map of Kerguelen Plateau and Broken Ridge showing ODP drill sites and major bathymetric features in the southeastern Indian Ocean (fine continuous line is 3000 m depth contour). ●, locations of Deep Sea Drilling Project and ODP drill sites. ▲, locations of dredge sites from which basaltic rocks have been recovered [see review by Coffin *et al.* (2000)].

Data are presented for major, trace, and volatile (H_2O, CO_2, S, Cl) element concentrations in 18 glass samples from Site 1140. These data are valuable for understanding the role of volatiles in the mantle source regions of these basalts, interpreting shallow-level magmatic processes, and inferring subsidence of the Northern Kerguelen Plateau following eruption of the basalts by using dissolved volatiles to estimate the paleo-eruption depths. The results also provide some insight into the release of S to the Earth's atmosphere during formation of the Kerguelen LIP.

GEOLOGICAL SETTING AND BASALT CHARACTERISTICS AT ODP SITE 1140

Site 1140 lies on the Northern Kerguelen Plateau (NKP) ~270 km north of the Kerguelen Archipelago (Fig. 1). The NKP is believed to have formed since 40 Ma as a result of Kerguelen hotspot magmatism (Royer & Sandwell, 1989; Royer & Coffin, 1992), and the Kerguelen Archipelago, which is part of the NKP, has volcanic rocks ranging in age from 39 Ma to recent (Nicolaysen *et al.*, 2000). Site 1140 lies at a depth of 2450 m on the northern flank of the NKP. The sediment sequence overlying basement is ~350 m thick. Drilling at Site 1140 penetrated 87·4 m of basement rocks, which were subdivided into six units (unit numbers increase downsection): five of the units are submarine basaltic flows (Units 1–3, 5, 6) and the sixth is a layer of dolomitized nannofossil chalk of ~1 m thickness (Unit 4; Coffin *et al.*, 2000). The basalts have been dated at 34 Ma (Duncan, 2002), consistent with biostratigraphic data (Coffin *et al.*, 2000). At this time, Site 1140 was ⩽50 km away from the SEIR axis (Royer & Sandwell, 1989).

Basement Units 1 and 6 each contain a massive lobe of ~5 m thickness in addition to ~30 small (50–100 cm) basaltic pillows (Coffin *et al.*, 2000). Only pillows of <1 m diameter were recovered from Units 2 and 3. Unit 5 contains similar pillows and a massive lobe of ~10 m thickness. Vesicularity varies within the units but is consistently low (<1–3 vol. %), and vesicles are largely restricted to chilled margins. Pillow margins are fine grained with unaltered glassy rims of 1–2 cm width. Unaltered glass is relatively abundant in Units 1 and 6 but rare in Units 2 and 3 and absent in Unit 5. Olivine is a minor phenocryst and groundmass phase in Units 1 and 2, but it is rare to absent in the lower basaltic units, in which clinopyroxene is a phenocryst phase. Units 4 and 6 are moderately plagioclase-phyric, whereas the others are essentially aphyric, with <1% phenocrysts in the massive portions of the flows. Major and trace element, and Sr–Nd–Pb isotope data for whole-rock pillow interior samples from Site 1140 have been presented by Weis & Frey (2002).

ANALYTICAL METHODS

Sample preparation

For IR spectroscopic analysis, millimeter-sized glass chips were selected that were visually free of alteration or

hair-like tubules that are the result of microbial alteration (Fisk *et al.*, 1998). The chips were mounted on glass slides using acetone-soluble, thermal-setting cement and ground into doubly polished wafers with two parallel sides. The thickness of each glass wafer was measured using a micrometer with a precision of ± 2 μm.

Infrared spectroscopy

Transmission IR spectra of the glasses were obtained using a Nicolet Magna 560 Fourier transform IR spectrometer interfaced with a Spectra-Tech Nic-Plan microscope in the Department of Geology and Geophysics at Texas A&M University. For each glass sample, two to three individual spectra were taken from different regions of the glass wafer using a circular aperture of 100 μm diameter. All spectra were taken using a KBr beamsplitter and liquid-nitrogen-cooled $HgCdTe_2$ (MCT) detector.

The quantitative procedures and band assignments described by Dixon *et al.* (1995) were followed for this work. Quantitative measurements of dissolved total H_2O, molecular H_2O, and carbonate (CO_3^{2-}) were determined using Beer's law:

$$c = \frac{(\text{m.w.}) \times (\text{abs.})}{\rho \times d \times \varepsilon}$$

where c is the concentration (in weight fraction) of the absorbing species, m.w. is the molecular weight (18·02 for total H_2O and molecular H_2O; 44·00 for CO_3^{2-}), abs. is the absorbance intensity of the band of interest, ρ is the room temperature density of the glass, d is the thickness, and ε is the molar absorption coefficient.

Total dissolved H_2O was measured using the intensity of the broad, asymmetric band centered at 3530 cm^{-1}, which corresponds to the fundamental OH-stretching vibration (Nakamoto, 1978). The absorbance intensity (peak height) was measured graphically from printed spectra, and the total H_2O concentration calculated using an absorption coefficient of 63 ± 3 L/mol cm (P. Dobson *et al.*, unpublished data; cited by Dixon *et al.*, 1995). Total water contents are listed in Table 1.

To examine the speciation of water in these glasses as a means of screening for low-temperature hydration, concentrations of dissolved molecular H_2O were measured using the intensity of the 1630 cm^{-1} absorption band, which corresponds to the fundamental bending mode of dissolved water molecules (Nakamoto, 1978). Unlike the molar absorptivity for the 3530 cm^{-1} band, which is relatively independent of composition for basaltic glasses, Dixon *et al.* (1995) have shown that the molar absorptivity for molecular water is compositionally dependent. Using the method described by Dixon *et al.* (1995) together with the average major element composition of the glasses, the molar absorptivity of the 1630 cm^{-1} band is 28 ± 2 L/mol cm.

Dissolved carbonate was measured from the absorbances of the bands at 1515 and 1430 cm^{-1}, which correspond to antisymmetric stretching of distorted carbonate groups (Fine & Stolper, 1986; Dixon *et al.*, 1995). Because the shape of the background in the region of the carbonate doublet is complex, absorbance intensities for the 1515 and 1430 cm^{-1} bands were measured after subtraction of a reference spectrum for a decarbonated basaltic glass so as to achieve a relatively flat background (Dixon *et al.*, 1995). The molar absorptivity for carbon dissolved as carbonate in basaltic glasses is compositionally dependent (Dixon & Pan, 1995). Dissolved carbonate contents (reported in Table 1 and hereafter as the equivalent amount of CO_2, in ppm) were determined using a molar absorption coefficient of 353 ± 7 L/mol cm, calculated from the average composition of the glasses and the linear equation reported by Dixon & Pan (1995).

Glass densities were calculated using major element analyses and the following partial molar volumes derived from density measurements of glasses at 1 bar and 25°C (R. Lange, personal communication, 2001): SiO_2 = $27{\cdot}01 \pm 0{\cdot}11$ (cm^3/mol), $Al_2O_3 = 37{\cdot}76 \pm 0{\cdot}38$, FeO = 10·5 (preliminary), MgO = $8{\cdot}81 \pm 0{\cdot}26$, CaO = $13{\cdot}03 \pm 0{\cdot}26$, $Na_2O = 19{\cdot}88 \pm 0{\cdot}29$, $K_2O = 33{\cdot}63 \pm 0{\cdot}49$, and $H_2O = 13{\cdot}93 \pm 0{\cdot}30$. Glass densities calculated with this model have a 1σ uncertainty of $\sim 0{\cdot}5\%$.

Electron microprobe

Major elements, S and Cl were analyzed in all glasses with a Cameca SX-50 electron microprobe at Texas A&M University using mineral and glass standards (Table 1). Analytical accuracy was assessed by analysis of US National Museum glass standard VG-2. Sulfur was analyzed using an anhydrite standard, 60 s on-peak counting time, and a S K_α wavelength offset measured on pyrite, which corresponds approximately to the $S^{6+}/\Sigma S$ ratio expected for a basaltic glass equilibrated at the fayalite–magnetite–quartz (FMQ) oxygen buffer (Wallace & Carmichael, 1994). Analyses of glass standard VG-2 using this procedure yielded a S concentration of $0{\cdot}137 \pm 0{\cdot}006$ wt % ($n = 11$), similar to the value reported by Dixon *et al.* (1991) and Dixon & Clague (2001). Sulfur analyses determined by these procedures are consistent with those measured by electron probe in mid-ocean ridge basalt (MORB) and seamount glasses (Wallace & Carmichael, 1992), based on interlaboratory comparisons. Chlorine was analyzed using procedures similar to those described by Michael & Cornell (1998). The electron beam was set at 15 kV, 100 nA, and a beam diameter of ~ 20 μm. Counting times were 200 s on peak and 200 s on background for each analyzed spot. The values reported in Table 1 are the averages of

Table 1: Major, trace, and volatile element concentrations in basaltic glasses from Site 1140

Sample:	26R-1, 3–4	26R-1, 85	26R-2, 89	27R-1, 70	27R-4, 126	27R-5, 69	28R-1, 140	28R-2, 35	28R-3, 86	31R-1, 37	31R-1, 65
Unit:	1	1	1	1	1	1	1	1	1	2	2
SiO_2	48·86	48·69	48·71	48·92	48·79	48·63	48·74	48·72	48·86	49·58	49·45
TiO_2	1·52	1·53	1·50	1·58	1·51	1·42	1·54	1·55	1·54	3·16	3·07
Al_2O_3	14·98	14·87	14·97	15·08	14·96	14·98	14·91	14·86	14·88	13·02	13·02
FeO^T	11·69	11·80	11·70	11·67	11·78	11·78	11·69	11·59	11·86	14·57	14·69
MnO	0·21	0·20	0·20	0·21	0·21	0·19	0·21	0·18	0·20	0·24	0·23
MgO	7·59	7·63	7·64	7·56	7·66	7·58	7·56	7·54	7·55	5·10	5·05
CaO	12·29	12·32	12·43	12·32	12·31	12·41	12·34	12·20	12·31	9·79	9·78
Na_2O	2·68	2·68	2·70	2·66	2·73	2·62	2·66	2·74	2·70	2·75	2·91
K_2O	0·17	0·16	0·16	0·18	0·16	0·17	0·17	0·17	0·17	0·66	0·67
P_2O_5	0·12	0·09	0·12	0·11	0·11	0·11	0·13	0·11	0·13	0·33	0·34
S	0·134	0·128	0·142	0·124	0·125	0·128	0·137	0·124	0·137	0·151	0·148
H_2O	0·25	0·23	0·24	0·26	0·23	0·26	0·25	—	0·26	0·43	0·44
CO_2 (ppm)	55	43	48	45	42	45	45	—	48	34	29
Cl (ppm)	42	—	—	—	48	—	50	—	46	146	152
Total	100·48	100·32	100·51	100·68	100·56	100·28	100·33	99·81	100·58	99·79	99·77
mg-no.	57·7	57·6	57·8	57·6	57·7	57·4	57·6	57·7	57·2	42·4	41·9
V	418	420	422	417	419	427	405	406	428	491	516
Cr	491	494	491	497	498	505	478	479	495	66	65·7
Sr	131	135	133	132	133	136	125	128	135	238	248
Y	35	35	35	35	35	36	33	34	36	44	46
Zr	93	93	92	84	92	93	79	86	93	207	230
Nb	3·5	3·4	3·7	3·0	3·5	3·6	2·7	3·1	3·8	15·9	20·3
Ba	36	37	37	35	36	38	32	35	37	136	147
La	3·6	3·5	3·6	3·6	3·7	3·8	3·5	3·7	3·5	15·5	14·5
Ce	11	11	12	11	11	12	11	11	12	43	44
Nd	9·8	9·8	9·1	9·5	9·7	9·3	9·2	9·9	9·5	24·9	23·1
Sm	3·5	3·8	3·1	3·0	3·2	3·1	3·1	3·3	2·9	6·3	5·5
Eu	1·2	1·4	1·3	1·4	1·2	1·3	1·3	1·4	1·1	2·4	2·1
Dy	5·4	4·9	5·1	5·0	4·6	5·0	5·1	5·1	4·7	6·5	6·6
Er	3·1	2·8	3·0	3·1	3·0	2·8	2·9	3·7	2·6	3·9	3·3
Yb	2·8	4·1	3·0	2·9	3·0	3·1	2·8	3·0	2·6	3·8	3·3

Sample:	32R-3, 42	34R-4, 96	34R-5, 56	34R-6, 64	35R-1, 60	35R-2, 136	35R-3, 57	36R-1, 0	36R-2, 48	37R-2, 46
Unit:	3	6	6	6	6	6	6	6	6	6
SiO_2	50·14	49·44	49·47	49·42	49·49	49·35	49·46	49·33	49·25	49·32
TiO_2	3·52	1·71	1·67	1·67	1·67	1·74	1·70	1·76	1·71	1·64
Al_2O_3	13·03	13·71	13·84	13·75	13·79	13·72	13·76	13·72	13·74	13·77
FeO^T	14·61	13·39	13·24	13·35	13·23	13·16	13·24	13·44	13·28	13·40
MnO	0·23	0·23	0·23	0·23	0·24	0·21	0·23	0·22	0·22	0·24
MgO	4·67	6·60	6·61	6·56	6·56	6·58	6·53	6·59	6·54	6·60
CaO	9·14	11·59	11·78	11·76	11·75	11·67	11·67	11·76	11·70	11·72
Na_2O	2·32	2·84	2·85	2·86	2·86	2·85	2·83	2·84	2·86	2·86
K_2O	0·89	0·20	0·17	0·18	0·18	0·18	0·18	0·18	0·18	0·19
P_2O_5	0·42	0·13	0·14	0·13	0·14	0·13	0·13	0·13	0·14	0·13
S	0·153	0·142	0·143	0·145	0·142	0·138	0·144	0·142	0·145	0·143
H_2O	0·69	—	0·27	0·27	0·26	—	0·26	0·26	0·26	0·26
CO_2 (ppm)	<20	—	35	35	41	—	34	37	46	38
Cl (ppm)	206	—	—	40	44	—	50	54	—	—
Total	99·82	99·99	100·41	100·33	100·31	99·72	100·13	100·38	100·03	100·26
mg-no.	40·1	50·9	51·2	50·8	51·0	51·2	50·8	50·7	50·8	50·8
V	509	440	461	458	452	446	450	456	456	451
Cr	58·5	113	120	116	113	117	111	116	114	113
Sr	241	125	132	130	130	127	126	130	131	128
Y	49	36	38	37	38	36	36	37	37	37
Zr	260	92	99	98	97	90	96	99	97	97
Nb	23·7	4·6	5·0	4·8	5·0	4·1	5·0	5·0	5·1	4·9
Ba	170	39	41	42	41	39	41	41	41	40
La	19·9	4·2	4·5	4·5	4·3	4·7	4·3	4·3	4·5	4·4
Ce	55	13	14	15	14	14	14	13	14	14
Nd	31·6	10·2	10·5	10·4	9·5	10·5	9·6	10·1	10·2	10·0
Sm	7·6	3·1	3·6	3·4	2·8	3·4	3·4	3·3	3·0	3·3
Eu	2·8	1·4	1·4	1·4	1·1	1·4	1·2	1·3	1·3	1·2
Dy	7·7	4·9	5·6	5·6	4·3	5·6	4·4	5·2	5·3	5·2
Er	4·8	3·0	3·2	3·2	2·5	3·5	2·7	3·2	3·0	3·2
Yb	4·4	2·9	3·4	3·4	2·5	3·3	2·5	3·0	3·3	3·0

Major elements (wt %), S (wt %), and Cl (ppm) were analyzed by electron microprobe at Texas A&M University. The values reported are averages of five analyses of each glass sample. One standard deviation uncertainties based on replicate analyses are equal to the following amounts, in wt %: SiO_2, 0·17; TiO_2, 0·08; Al_2O_3, 0·08; FeO, 0·15; MnO, 0·02; MgO, 0·06; CaO, 0·10; Na_2O, 0·06; K_2O, 0·01; P_2O_5, 0·02; S, 0·008; Cl, 0·001. H_2O (wt %) and CO_2 (ppm) were determined by Fourier transform IR spectroscopy (FTIR) using methods described in the text. The reported values are averages of two or more spectra of a single glass chip, and in some cases, averages of spectra from two chips from a single pillow rim. Most glasses have molecular H_2O (1630 cm^{-1}) below detection, consistent with high-temperature equilibrium for basaltic melts with low total H_2O (Dixon *et al.*, 1995). The more H_2O-rich Unit 3 glass has 0·06 wt % molecular H_2O, which also agrees with the high-temperature equilibrium curve. Only two spectra showed molecular H_2O in excess (by 0·05–0·2 wt %) of that expected for high-temperature equilibrium, probably as a result of low-temperature hydration. These spectra also have higher total H_2O than other spots within the same glass chip or another chip from the same pillow rim. The values affected by hydration were not included in the reported averages. *mg*-number is calculated assuming 85% of total Fe is present as FeO. Trace elements (ppm) were analyzed by ion microprobe at Woods Hole Oceanographic Institution using techniques described in the text. One standard deviation uncertainties are equal to the following percentages of the amount present: V, 2%; Cr, 2%; Sr, 2%; Y, 2%; Zr, 5%; Nb, 9%; Ba, 4%; La, 3%; Ce, 3%; Nd, 3%; Sm, 7%; Eu, 8%; Dy, 6%; Er, 10%; Yb, 13%).

analyses of five spots on each glass chip. Precision for the analyses was ± 8 ppm (1σ). Analyses of olivine consistently yielded ~ 10 ppm Cl. Following Michael & Cornell (1998), values reported in Table 1 have been corrected by subtracting this 'blank' value from the raw microprobe value.

Ion microprobe

Abundances of rare earth elements (REE: La, Ce, Nd, Sm, Eu, Dy, Er, Yb) and other trace elements (V, Cr, Sr, Y, Zr, Nb, Ba) were determined with a Cameca IMS 3f ion microprobe at Woods Hole Oceanographic Institution using procedures described by Shimizu (1998). The energy filtering technique (Shimizu & Hart, 1982) was used to suppress molecular ion interferences by offsetting the secondary accelerating voltage by 60 V for REE and by 90 V for other elements. Element abundances were determined from secondary ion intensity (ratioed against that of silicon) using empirical relationships between intensity and concentration. Analytical uncertainties (1σ) based on replicate analyses are 3–13% for REE and 2–9% for the other elements (Table 1). Average trace element abundances for glasses from each unit were compared with whole-rock analyses of pillow interiors (Weis & Frey, 2002). After correcting for the effect of phenocrysts in the whole-rock samples (Michael, 1995), average differences between glass and whole rock for incompatible trace elements are as follows: Y (–3%), Zr (–1%), Nb (5%), Ba (22%), La (–11%), Ce (5%), Nd (–6%), Sm (–12%), Eu (–2%), Dy (–16%), Er (–13%), Yb (–9%). Such a comparison cannot be made for V, Cr, and Sr because they are compatible in phenocryst phases in the pillow interiors.

RESULTS

Nine glass samples from each of Units 1 and 6 were analyzed for major and trace elements. Fresh glass is rare in Units 2 (two samples analyzed) and 3 (only one sample analyzed). Glasses from all units are tholeiitic in composition on the basis of total alkalis vs SiO_2. Within both Units 1 and 6, glasses are homogeneous in major element composition, mostly within the precision of the electron probe analyses, but there are significant differences between the two units (Fig. 2). On the basis of the homogeneity of analyzed glass compositions, flow units 1 and 6 probably each represent an individual eruptive episode. Average MgO contents are 7·6 wt % for Unit 1 and 6·6 wt % for Unit 6. Unit 1 and 6 glasses are similar in major element composition to glasses from the Southeast Indian Ridge (SEIR) away from the Amsterdam–St. Paul Platform (Fig. 2; Douglas Priebe, 1998).

Unit 2 and 3 glasses are more differentiated (5·1 and 4·7 wt % MgO, respectively) than those of Units 1 and 6 (Fig. 2). Glasses from Units 2 and 3 have significantly higher K_2O/TiO_2, a ratio that increases with degree of source region enrichment (e.g. Nb/Zr or La/Sm), than Unit 1 and 6 glasses. Crystal fractionation modeling indicates that Units 2 and 3 evolved from parental magmas with higher concentrations of K_2O, TiO_2, and P_2O_5 than the magmas represented by Units 1 and 6 (Fig. 2). The Unit 2 and 3 glasses are similar in major element composition to the most differentiated glasses recovered from the SEIR along the ASP platform (Fig. 2). They also have compositional similarities to some 29–30 Ma subaerial flood basalts from the Kerguelen Archipelago, but in general the flood basalts are even more highly differentiated (Fig. 2).

Incompatible trace element abundances of Unit 6 glasses are slightly greater than those of Unit 1, whereas Units 2 and 3 are much more highly enriched, with incompatible trace element abundances ranging from 10 to 30 times greater than primitive mantle values (Fig. 3). For Units 2 and 3, strong depletion of Sr relative to Nd suggests extensive plagioclase fractionation, consistent with their highly differentiated (low MgO and Al_2O_3) compositions. In incompatible trace element ratio diagrams (Fig. 4), Unit 1 glasses are similar in composition to SEIR MORB, and Unit 2 and 3 glasses are transitional between SEIR MORB and Kerguelen Archipelago flood basalts whose Sr–Nd–Pb isotopic compositions are believed to be representative of the Kerguelen plume (Yang *et al.*, 1998). Unit 6 glasses are slightly more enriched than SEIR MORB. Thus the trace element patterns indicate an order of increasing enrichment Unit 1 < Unit 6 < Unit 2 < Unit 3. Sr–Nd–Pb isotope data confirm these patterns (Weis & Frey, 2002), and demonstrate that Units 2 and 3 are derived from mixtures of Kerguelen plume and MORB (asthenospheric) mantle.

Concentrations of H_2O are very uniform for glasses within Units 1 and 6 (Fig. 5), consistent with the interpretation from the major element data that the multiple glass-rimmed pillows within each flow unit represent an individual eruptive episode. Average values in wt % H_2O for Units 1 and 6 are $0{\cdot}25 \pm 0{\cdot}01$ and $0{\cdot}26 \pm 0{\cdot}01$, respectively. H_2O contents of the enriched glasses are significantly higher, with values of 0·44 wt % for Unit 2 and 0·69 wt % for Unit 6. Dissolved CO_2 concentrations are relatively low in all samples (Fig. 5), with values of 42–55 ppm (Unit 1), 29–34 ppm (Unit 2), <20 ppm (Unit 3), and 34–46 ppm (Unit 6). Vapor saturation pressures [based on Dixon *et al.* (1995)] for glasses in Units 2 and 6 are slightly lower (average 87 ± 8 bars) than those for Unit 1 (average 106 ± 9 bars). The maximum vapor saturation pressure for the single Unit 3 glass sample is 90 bars, based on CO_2 <20 ppm.

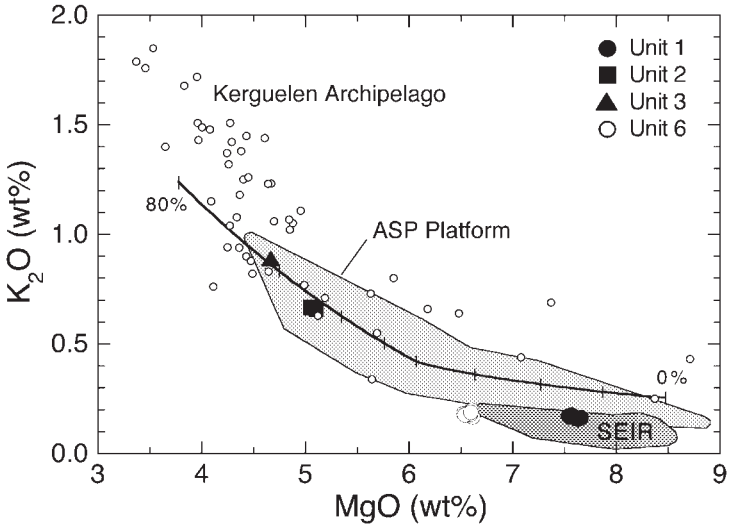

Fig. 2. MgO vs K_2O for basaltic glasses from Site 1140. For comparison, the small open circles show the compositions of 29–30 Ma subaerial flood basalts on the Kerguelen Archipelago (Yang *et al.*, 1998). Gray shaded fields show the range of compositions erupted along the Southeast Indian Ridge both away from (SEIR) and on (ASP) the Amsterdam–St. Paul Platform (Douglas Priebe, 1998). Bold continuous line shows a calculated (Ariskin *et al.*, 1993) 1 bar liquid line of descent for an MgO-rich Kerguelen Archipelago lava to illustrate how K_2O varies with extent of crystal fractionation. Vertical tick marks along the line indicate 10% increments of crystallization.

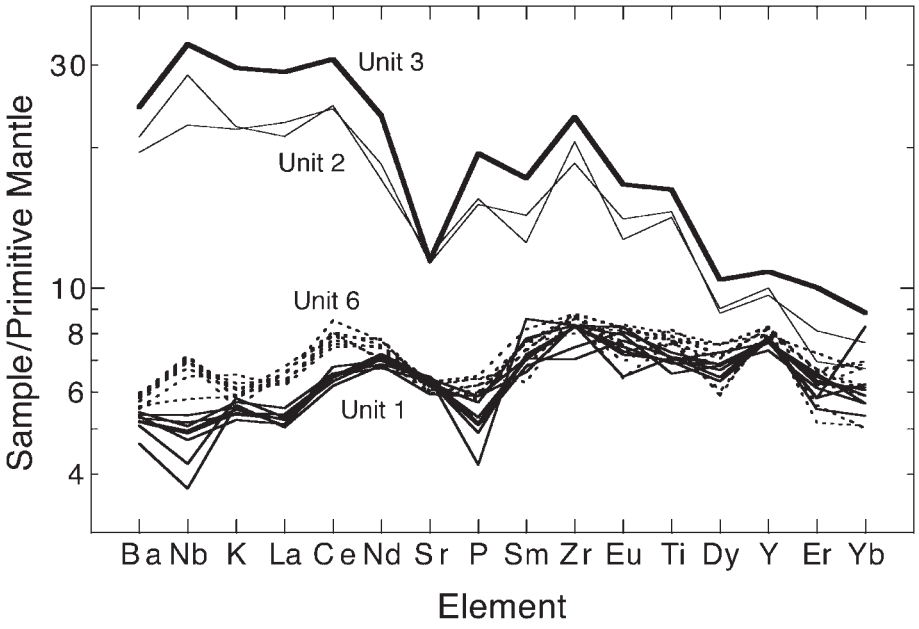

Fig. 3. Trace element abundances in basaltic glasses from Site 1140. Concentrations for each element are normalized to primitive mantle values (Sun & McDonough, 1989).

Because H_2O in basaltic magmas behaves as an incompatible element during partial melting and crystal fractionation (Moore, 1970), it is useful to compare H_2O variations with other incompatible elements (Fig. 6). The H_2O/K_2O ratios of Unit 1 and 6 glasses are similar to published analyses of SEIR glasses (Michael, 1995) and to glasses with Indian Ocean-type mantle trace element characteristics recovered from ODP Leg 187 drill sites located near the SEIR at the Australian–Antarctic Discordance. Unit 2 and 3 basaltic glasses have lower H_2O/K_2O than those from Units 1 and 6 (Fig. 6), but the Unit 3 glass has similar H_2O/K_2O to E-MORB from near-ridge seamounts on the East Pacific Rise (Michael, 1995).

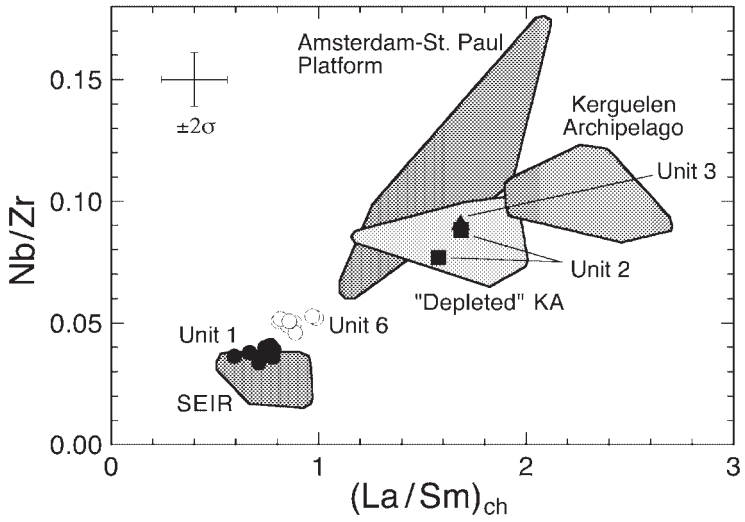

Fig. 4. La/Sm (chondrite normalized) vs Nb/Zr for basaltic glasses from Site 1140 (symbols as in Fig. 2). The shaded fields show the range of variation for SEIR MORB lavas away from and on the Amsterdam–St. Paul Platform, 29–30 Ma subaerial flood basalts on the Kerguelen Archipelago (Yang *et al.*, 1998), and 'depleted' Kerguelen Archipelago basalts [Group D of Yang *et al.* (1998)]. It is important to note that Unit 2 and 3 glasses do not share certain geochemical characteristics, such as anomalously high Sr/Nd, with the Group D lavas.

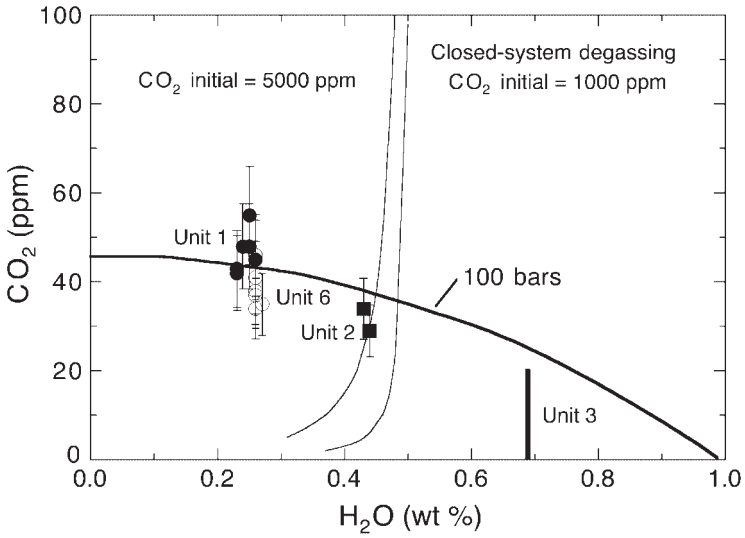

Fig. 5. H_2O vs CO_2 for basaltic glasses from Site 1140 (symbols as in Fig. 2). The CO_2 content of the single glass sample from Unit 3 is below the detection limit of ~20 ppm, as indicated by the vertical bar. Shown for reference is a vapor saturation curve for 100 bars pressure calculated using solubility data from Dixon *et al.* (1995). Closed-system degassing curves for basaltic melt with 0·5 wt % initial H_2O and 1000 and 5000 ppm CO_2 are calculated based on Dixon & Stolper (1995).

Sulfur concentrations for glasses in Units 1 and 6 average 1310 ± 70 and 1430 ± 20 ppm S, respectively. On a diagram of FeO^T vs S (Fig. 7), the values for Unit 1 are similar to SEIR MORB glasses with ~12 wt % FeO^T. The Unit 6 glasses are slightly more Fe rich, but have S contents within the range of MORB values worldwide. The S content of MORB glasses is usually controlled by saturation with immiscible Fe–S–O liquid (Wallace & Carmichael, 1992), so the similarity of Unit 1 and 6 glasses to MORB values suggests that they were sulfide liquid saturated at the time of eruption. Sulfur contents of the enriched (Units 2 and 3) glasses are higher than for Units 1 and 6. The enriched glasses are also more evolved (higher FeO^T), and they fall near the MORB sulfide saturation curve and within the range for MORB glasses in general (Fig. 7).

Chlorine contents of the Unit 1 and 6 glasses are very low (40–55 ppm), and within the range for SEIR MORB

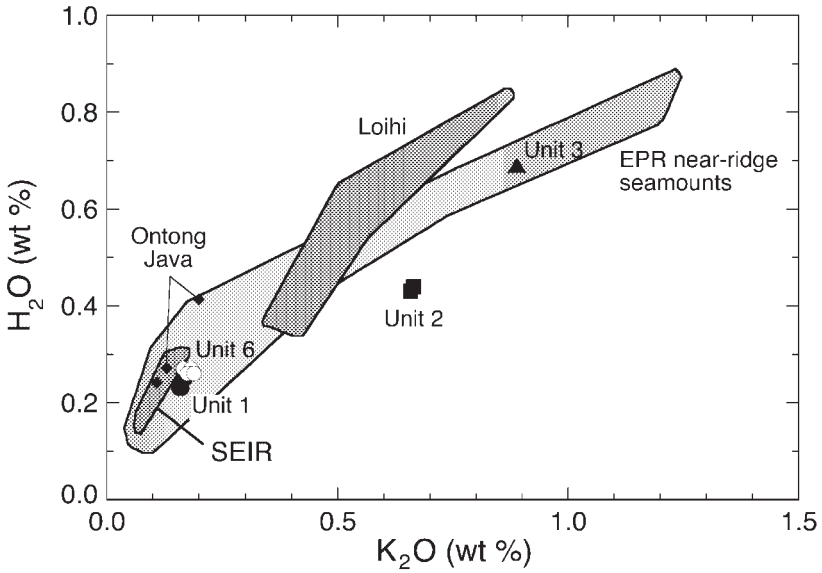

Fig. 6. H_2O vs K_2O for basaltic glasses from Site 1140 (symbols as in Fig. 2). Shown for comparison are the ranges of data for the SEIR, Loihi Seamount, and near-ridge seamounts from the East Pacific Rise (EPR; Michael, 1995). The SEIR data field includes analyses (P. J. Wallace, unpublished data, 2001) for glasses with Indian Ocean-type trace element characteristics from the SEIR at the Australian–Antarctic Discordance (ODP Leg 187). Also shown (◆) are averages for glasses from ODP Sites 803 (average for all glasses) and 807 (averages for two different compositional types) on the Ontong Java Plateau (Michael, 1999). For the Site 1140 glasses, $\pm 2\sigma$ uncertainty is approximately equal to the symbol size.

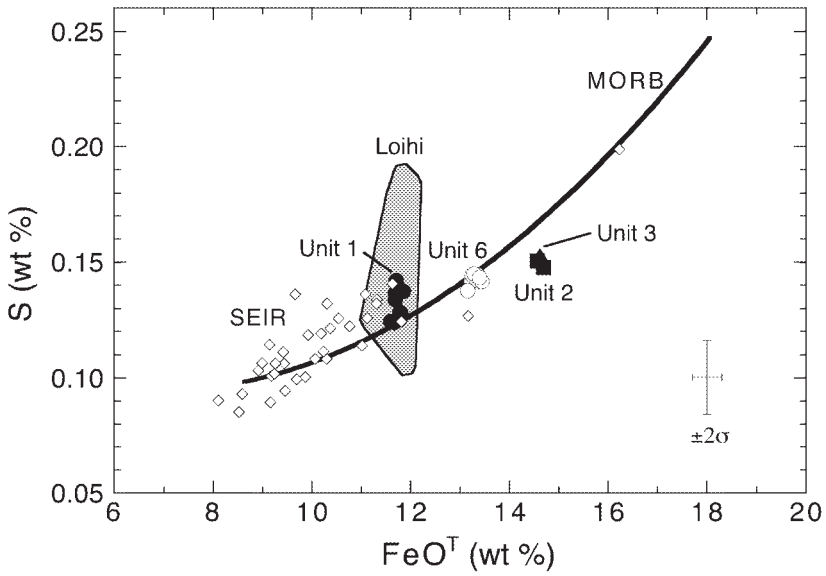

Fig. 7. FeO^T vs S for basaltic glasses from Site 1140 (symbols as in Fig. 2). For comparison, SEIR glasses are shown by small open diamonds (Douglas Priebe, 1998). Field for Loihi Seamount and curve for MORB are based on data from Wallace & Carmichael (1992).

(Fig. 8). The enriched glasses have higher Cl, with concentrations of ~150 ppm Cl for Unit 2 and 206 ppm for Unit 3. Like H_2O, Cl behaves as an incompatible element during partial melting in the mantle and crystallization of basaltic magmas (Schilling *et al.*, 1980). Variations in Cl can therefore be best understood by comparing them with other incompatible elements such as K. Cl/K ratios are relatively low (0·03–0·04) for all Site 1140 glasses (Fig. 9). This ratio is sensitive to assimilation of hydrothermally altered material (Michael & Cornell, 1998), and Cl/K varies from below detection limits (~0·01) in normal MORB to ~0·07 in enriched MORB magmas that have not been affected by assimilation. The low values for Site 1140 glasses from all

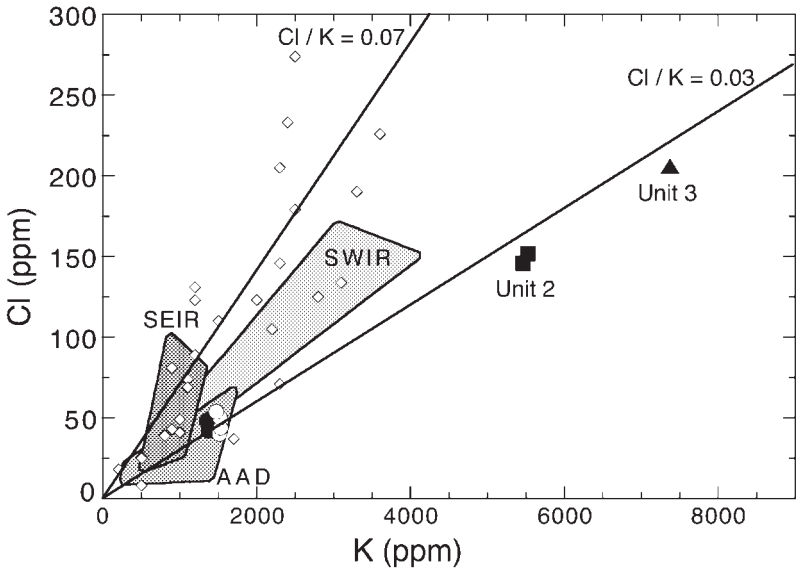

Fig. 8. K vs Cl for basaltic glasses from Site 1140 (symbols as in Fig. 2). SEIR glass data shown by the gray field are from Michael & Cornell (1998) whereas individual glass analyses from Douglas Priebe (1998) are shown by small open diamonds. Southwest Indian Ridge (SWIR) and Australian–Antarctic Discordance (AAD) glass data shown as gray fields are also from Michael & Cornell (1998). Cl/K values of 0·03 and 0·07 are the approximate endmember limits for depleted and enriched MORB, respectively (Michael & Cornell, 1998). For the Site 1140 glasses, $\pm 2\sigma$ uncertainties in Cl analyses are about twice the symbol size.

units indicate that such assimilation did not occur during shallow-level crystallization (Fig. 9). Interestingly, it has been shown that for some submarine oceanic islands (Loihi) and LIPs (Ontong Java Plateau), assimilation of material with a seawater-derived component resulting in high magmatic Cl contents appears to be a widespread phenomenon (Kent *et al.*, 1999*a*, 1999*b*; Michael, 1999).

DISCUSSION

Pressures of crystallization

The pressures of phenocryst formation in Site 1140 magmas can be estimated by comparing experimental phase equilibrium results with the phenocryst assemblage that is present in each of the basalt units (Fig. 10). Basalt in Unit 1 contains phenocrysts of olivine + plagioclase. These phases are predicted to be on the liquidus of a melt with the glass composition at pressures ≤ 4 kbar based on calculations using the methods of Ariskin *et al.* (1993) and Yang *et al.* (1996). Unit 2 basalts contain phenocrysts of olivine + plagioclase + augite, an assemblage that would be on the liquidus for this composition only at pressures <1 kbar (see Fig. 10). Basalts in Unit 3 are relatively aphyric, with sparse phenocrysts of olivine + plagioclase. The absence of augite indicates a crystallization pressure of <1 kbar for the phenocrysts. Despite the absence of augite in the phenocryst assemblage, the relatively low Sc abundances in whole-rock samples from Unit 3 indicate an important role for augite fractionation (Weis & Frey, 2002). Unit 6 basalt contains phenocrysts of plagioclase + augite + minor olivine. This assemblage would be on the liquidus at a pressure of 1·5 kbar (Fig. 10), suggesting a relatively low pressure of crystallization before eruption, similar to that inferred for basaltic magmas represented by Units 2 and 3. Unit 2 and 3 basaltic magmas have undergone more extensive crystal fractionation (4·6–5·1 wt % MgO) than Units 1 and 6, and the phase equilibrium results in Fig. 10 indicate that fractionation occurred at relatively low pressure (≤ 1 kbar).

Volatiles in mantle source regions for Kerguelen Plateau basaltic magmas

Ocean island basaltic magmas are enriched in H_2O relative to depleted MORB, giving rise to the possibility that the excess magmatism associated with mantle plumes is caused, at least in part, by the effect of higher H_2O on mantle melting rather than solely being due to high mantle potential temperature (Schilling *et al.*, 1980; Bonatti, 1990). A greater H_2O content for the lower mantle, from which mantle plumes probably derive (Hofmann, 1997), could indicate the involvement of undegassed primitive mantle (based on high $^3He/^4He$) or could result from recycling of subducted oceanic crust and sediments into the lower mantle. However, despite the higher

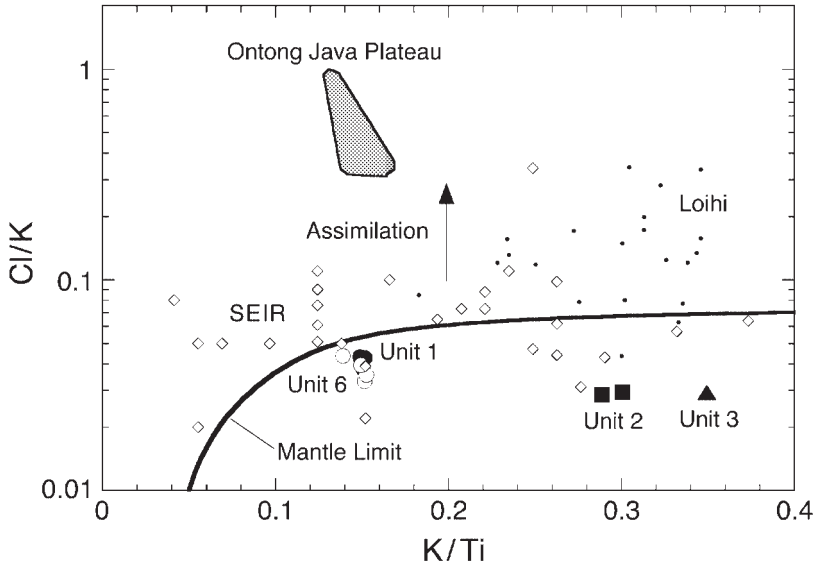

Fig. 9. K/Ti vs Cl/K for basaltic glasses from Site 1140 (symbols as in Fig. 2). (Note that the vertical axis is a log scale.) SEIR glass data (Douglas Priebe, 1998) are shown as small open diamonds. Small filled circles are data for pillow-rim glasses and olivine-hosted melt inclusions from Loihi Seamount (Kent *et al.*, 1999*a*, 1999*b*). Field for Ontong Java Plateau submarine glasses is from Michael (1999). The effect of assimilation involving altered rocks with a seawater-derived component is shown by the vertical arrow. The line labeled 'mantle limit' is a calculated mixing curve between enriched and depleted MORB endmembers that have not been affected by assimilation (Michael & Cornell, 1998).

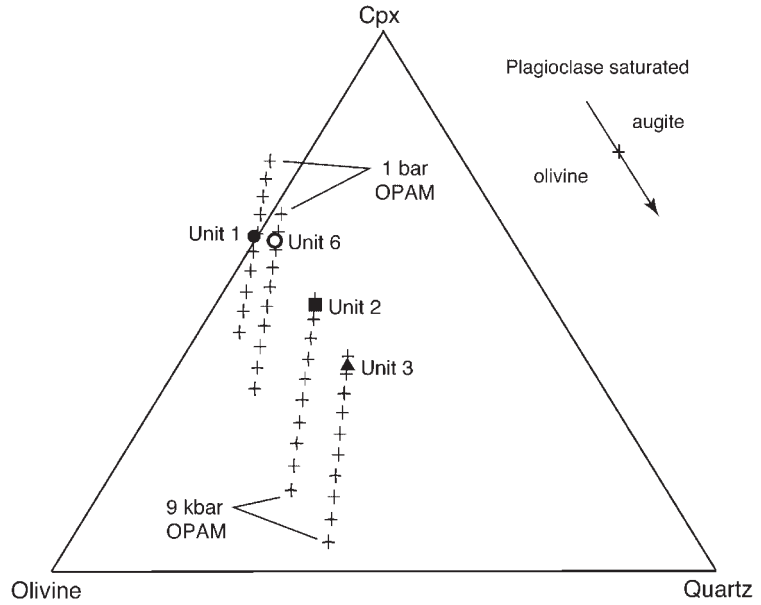

Fig. 10. Prediction of pressures at which melts coexist with olivine + plagioclase + augite. The average major element compositions of glasses from Units 1, 2, 3, and 6 are recalculated into normative oxygen unit components and projected from plagioclase onto the olivine–clinopyroxene–quartz plane (Yang *et al.*, 1996). For each of the four average compositions, the near-vertical line of plus symbols shows the point at which melt is predicted to coexist with olivine + plagioclase + augite at pressures ranging from 1 bar (uppermost plus symbol) to 9 kbar (lowermost plus symbol), in increments of 1 kbar (Yang *et al.*, 1996). The topology of the olivine + augite + plagioclase cotectic at any given pressure is shown schematically at upper right.

H_2O content of mantle-plume-related basaltic magmas, a recent study of Loihi Seamount, Hawaii, has shown that H_2O is depleted relative to Ce, an element of similar incompatibility (Dixon & Clague, 2001). These data have been interpreted to indicate that the recycled oceanic crustal (+ sediment) component in the Hawaiian plume

is more depleted in H_2O than either the depleted upper-mantle source region for MORB or primitive undegassed mantle (Dixon & Clague, 2001).

Before using the Site 1140 glasses to constrain mantle volatile contents of the Kerguelen plume, it is important to ascertain whether significant H_2O was lost by degassing before eruption and quenching of the glass. Closed-system degassing calculations suggest that for the Unit 1, 2, and 6 glasses, no more than ~10% of the original primary H_2O could have been lost by degassing, even if the primary magmas had a relatively high initial CO_2 content (Fig. 5). In contrast, the Unit 3 glass sample, with its higher H_2O content, is much closer to the saturation value for pure H_2O-vapor at the inferred eruption and quenching pressure of ~90 bars. This, coupled with very low CO_2, makes it a possibility that significant H_2O was lost by degassing during shallow-level crystallization or submarine eruption. However, the low vesicularity (<3 vol. %) and relatively high S and Cl contents of the Unit 3 glass (similar to Unit 2 glasses) suggest that it has not lost a significant proportion of its initial H_2O by degassing. The relatively high S and MORB-like Cl contents of all Site 1140 glasses indicate that they have not been affected by the complex, partial degassing process that occurs in some oceanic islands that have both subaerial and submarine active regions (Dixon *et al.*, 1991).

Both depleted and enriched MORB from most regions of the world, except for the northern Mid-Atlantic Ridge and the SEIR, have average H_2O/Ce values of 160–210 (±40 for each regional average; Michael, 1995). Available data for SEIR MORB show anomalously high values (average $H_2O/Ce = 252$), and H_2O/Ce appears to increase with increasing $^{87}Sr/^{86}Sr$ (Fig. 11). Unit 1 glasses, which have Sr–Nd–Pb isotopic compositions within the range of SEIR MORB (Weis & Frey, 2002), have average H_2O/Ce of 216 ± 12 (1σ) and fall within the lower end of the range of H_2O/Ce and La/Sm for SEIR glasses. However, the Unit 1 glasses have higher $^{87}Sr/^{86}Sr$ than any of the SEIR glasses that have been analyzed for H_2O (Fig. 11). Unit 6 glasses, which are intermediate between SEIR MORB and Kerguelen plume in both trace element ratios (Fig. 2) and $^{87}Sr/^{86}Sr$ (Fig. 11b), have slightly lower H_2O/Ce than Unit 1 (average $H_2O/Ce = 186 \pm 6$). Units 2 and 3, which have trace element and isotopic characteristics closer to those of the Kerguelen plume, both have very low H_2O/Ce (100 and 126, respectively; Fig. 11). If the low H_2O/Ce of enriched glasses from Site 1140 is a general characteristic of basaltic magmas derived from the Kerguelen plume, then excess melting cannot be due to higher than normal mantle H_2O contents, and requires that melting of the plume occurs because of relatively high mantle potential temperature.

The Kerguelen plume component has Sr–Nd–Pb isotopic characteristics intermediate between EM-1 and EM-2 (Weis *et al.*, 1993). The EM sources reflect the presence of recycled material in the mantle, with EM-1 representing either recycled, ancient pelagic sediment or recycled, ancient subcontinental lithosphere and EM-2 representing recycled oceanic crust with a small amount of continent-derived sediment (see Hofmann, 1997, for review). The limited data for enriched glasses from Site 1140 (only three glassy margins from Units 2 and 3) are far too sparse to draw any firm conclusions about H_2O in the Kerguelen plume component. However, the results shown in Fig. 11 suggest the possibility that the recycled component in the Kerguelen plume source may be strongly depleted in H_2O relative to Ce, as has been suggested for the 'Koolau' component of the Hawaiian plume (Dixon & Clague, 2001).

Subsidence of the Kerguelen Plateau

The subsidence of oceanic plateaux is believed to result from cooling and contraction of the lithospheric plate on which the plateau is constructed (Detrick *et al.*, 1977). It was discovered during ODP Legs 119 and 120 that large parts of the Southern Kerguelen Plateau that are now submarine were originally subaerial during plateau construction. If the plateau had subsided at rates similar to normal oceanic lithosphere, then original maximum elevations would have been of the order of 1–2 km above sea level, and much of the southern plateau's ~500 000 km^2 area would at one time have been above sea level (Coffin, 1992).

A major source of uncertainty in assessing oceanic plateau subsidence is estimating original depth (e.g. using microfossils) or elevation above sea level at the time of eruption. Eruption depth estimates for basaltic pillow lavas can be made using dissolved CO_2 in glass rims (e.g. Dixon *et al.*, 1991) because of the strong pressure dependence of CO_2 solubility in basaltic melts. For Site 1140, the Unit 2 and 6 glasses suggest an eruption pressure of 87 bars (= 870 m below sea level), whereas Unit 1 glasses indicate a slightly higher pressure (~100 bars) that may result from slight CO_2 supersaturation (Fig. 5). The lack of detectable carbonate (<20 ppm CO_2) for Unit 3 glasses is consistent with an eruption pressure ⩽90 bars. The fact that dissolved CO_2 in glasses with very different H_2O contents from all four units gives generally consistent pressure estimates suggests that this pressure does not reflect strong CO_2 supersaturation (e.g. Dixon & Stolper, 1995). Assuming an original eruption depth of 870 m for the sequence at Site 1140 and taking account of the effect of sediment loading on subsidence (Crough, 1983), the estimated subsidence for the Northern Kerguelen Plateau is 1664 m (Fig. 12). This value is in excellent agreement with the prediction (~1700 m subsidence) for 34 Ma normal Indian Ocean lithosphere.

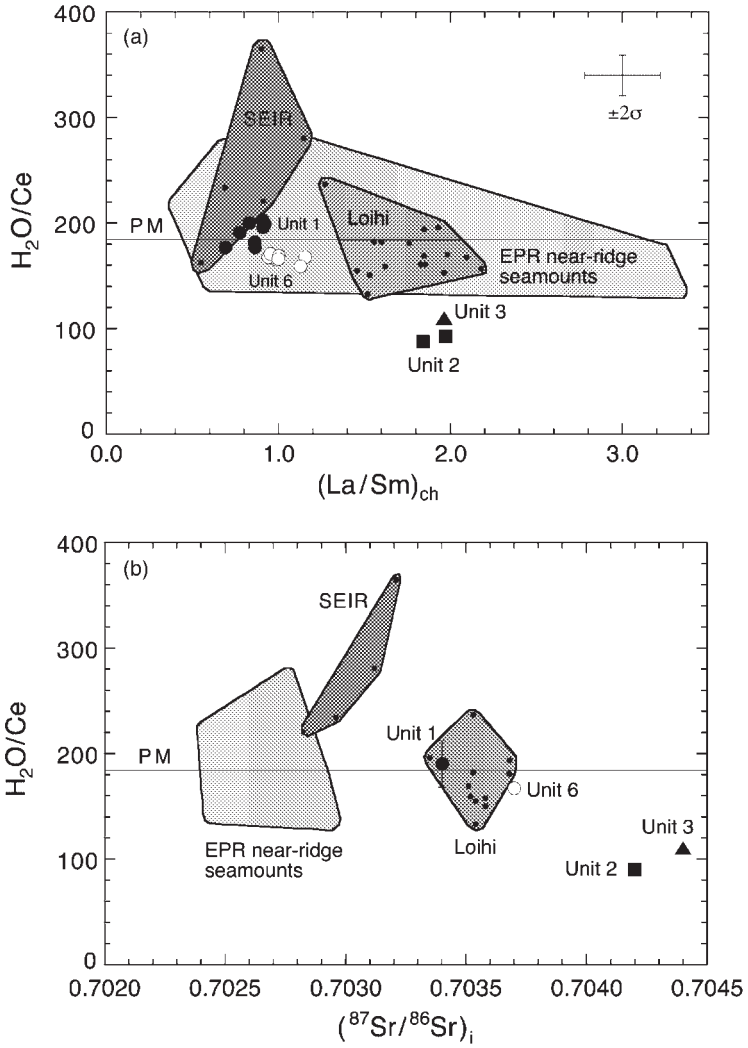

Fig. 11. H_2O/Ce vs chondrite-normalized La/Sm (a) and initial $^{87}Sr/^{86}Sr$ (b) for Site 1140 glasses. $^{87}Sr/^{86}Sr$ data for Site 1140 glasses are from Weis & Frey (2002) and are age corrected to 34 Ma. For the average values for Units 2 and 6 in (b), $\pm 2\sigma$ is slightly larger than the symbol size. SEIR data are from Dosso *et al.* (1988) and Michael (1995), EPR near-ridge seamount data are from Batiza & Vanko (1984) and Michael (1995), and Loihi Seamount data are from Michael (1995) and Dixon & Clague (2001). Line labeled 'PM' is the H_2O/Ce value for primitive mantle estimated by Dixon & Clague (2001).

Although subsidence estimates for the much older Central and Southern Kerguelen Plateau are more uncertain, they are also mostly consistent with expectations for normal oceanic lithosphere (Fig. 12).

The one site (Site 1139) that appears to have anomalous subsidence (Fig. 12) is located on Skiff Bank, a bathymetric and gravimetric high ~350 km WSW of the Kerguelen Archipelago (Fig. 1). Volcanic rocks recovered from Site 1139 have been dated at 69 Ma (Duncan, 2002), but Skiff Bank appears to be structurally related to the Northern Kerguelen Plateau, on which flood basalt eruptions occurred until ~25 Ma (Frey *et al.*, 2000). As a result, thermal subsidence of Skiff Bank might have been minimal for ~40 Myr after its formation due to dynamic uplift associated with the Kerguelen hotspot, thermal rejuvenation of the lithosphere, or a combination of the two. If it is assumed that the oldest bathyal sediments at Site 1139 were deposited at ~500 m water depth (a likely minimum for this type of sediment), then the estimated total subsidence is ~2200 m, which agrees well with predictions for normal oceanic lithosphere (Fig. 12).

Implications for volatile release to the environment

The eruption of enormous volumes of basaltic magma during formation of the Kerguelen Plateau and Broken

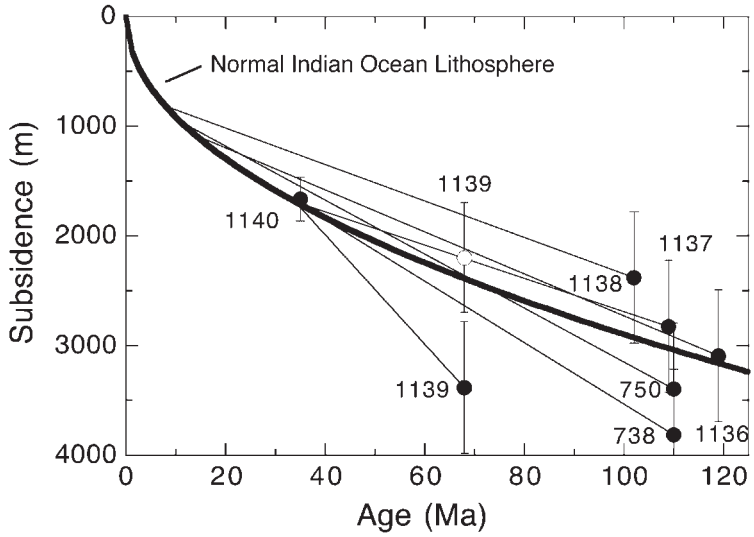

Fig. 12. Subsidence estimates for various parts of the Kerguelen Plateau plotted as a function of eruption age of basement basalts. The subsidence for Site 1140 is calculated using the average vapor saturation pressure for the analyzed glasses from Units 2 and 6 (see Fig. 5). For all other sites, the basement basalts were erupted in a subaerial environment, so there is no information on the original elevation above sea level at the time of eruption. Therefore, I have assumed that these other sites subsided like normal Indian Ocean lithosphere from the time of eruption until the time represented by the oldest marine sediments on top of basement. It should be noted that this assumption applies only to the first 10–20 Myr following subsidence. For each site, subsidence from the time of the oldest marine sediment to the present day is shown as a fine continuous line. ○, alternate subsidence model for Site 1139 in which it is assumed that the oldest bathyal sediments overlying basement were deposited at 500 m water depth. For reference, the bold continuous line shows the subsidence curve for normal Indian Ocean lithosphere (Hayes, 1988). Eruption ages were determined by $^{40}Ar/^{39}Ar$ dating (Pringle *et al.*, 1994; Duncan, 2002). Biostratigraphic ages are from Coffin *et al.* (2000) and references therein. For all sites, including Site 1140, the present-day depth of the top of igneous basement has been corrected for sediment loading (i.e. the actual present-day depth is greater than would have occurred as a result of thermal subsidence alone because of the additional effect of sediment loading). The corrected basement depth (D_c) is obtained from the equation of Crough (1983): $D_c = d_w + t_s(\rho_s - \rho_m)/(\rho_w - \rho_m)$, in which d_w is water depth in meters, t_s is sediment thickness in meters, ρ_s is average sediment density (1·90 g/cm^3), ρ_m is upper-mantle density (3·22 g/cm^3), and ρ_w is seawater density (1·03 g/cm^3).

Ridge probably had significant environmental consequences as a result of release of volatiles such as CO_2, S, Cl, and F. The fact that much of the plateau formed by subaerial volcanic eruptions (Coffin *et al.*, 2000; Coffin, 1992) is significant in this regard because basaltic magmas are nearly completely degassed during subaerial eruptions.

The magma output rate of the Kerguelen hotspot through time has been estimated by Coffin *et al.* (2002) based on radiometric dating and crustal structure determined from geophysical data and drilling results. The results suggest that the magma output rate between 95 and 120 Ma, when the Southern and Central Kerguelen Plateau and Broken Ridge were formed, was ~1 km^3/yr. The magma output rate appears to have decreased after that time (95 to ~25 Ma) to values of ~0·1 km^3/yr. Data for Unit 2 and 3 glasses at Site 1140 suggest that ~1400 ppm S would be degassed during subaerial eruption (Fig. 7). Assuming that 50% of the Southern and Central Kerguelen Plateau and Broken Ridge formed by subaerial eruptions (Coffin, 1992), then the S flux to the atmosphere from 120 to 90 Ma would have been 2×10^{12} g S/yr. This value is ~10% of the current global flux of S to the atmosphere from subaerial eruptions (Andres & Kasgnoc, 1998). Unfortunately, the Site 1140 glasses do not provide any information on the primary CO_2 contents of Kerguelen Plateau basaltic magmas because the relatively low inferred quenching pressures for the glasses indicate that most of the primary CO_2 has been degassed (Fig. 5).

An important factor that would have increased the environmental consequences of volcanic S release during formation of the Kerguelen Plateau is the high latitude at which the plateau formed (Frey *et al.*, 2000). In most basaltic eruptions, released volatiles remain in the troposphere, but at high latitudes, the tropopause is relatively low, allowing large mass flux basaltic fissure eruption plumes to transport SO_2 and other volatiles into the stratosphere (Stothers *et al.*, 1986; Self *et al.*, 1998). Sulfuric acid aerosol particles that form in the stratosphere after such eruptions have a longer residence time and greater global dispersal than if the SO_2 remains in the troposphere, resulting in greater effects on climate and atmospheric chemistry. The value of 2×10^{12} g S/yr estimated above for Kerguelen Plateau formation from 120 to 95 Ma is comparable in magnitude with the

current global estimate for mass of S injected annually into the stratosphere by explosive eruptions (Pyle *et al.*, 1996).

CONCLUSIONS

Submarine glassy pillow basalts (34 Ma) from the Northern Kerguelen Plateau (Site 1140) have La/Sm and Nb/Zr ratios that vary from values similar to SEIR MORB (Unit 1), to slightly more enriched (Unit 6), to values transitional between SEIR MORB and basaltic magmas formed by melting of the Kerguelen plume (Units 2 and 3). On the basis of comparison with experimental phase equilibria, basaltic magmas from most units (2, 3 and 6) appear to have crystallized at relatively low pressures (<1·5 kbar) before eruption, but crystallization of Unit 1 basalt may have occurred at higher pressures ($\leq$4 kbar). Volatile contents for glasses in Units 1 and 6 are similar to depleted MORB values but are significantly higher for the enriched glasses (Units 2 and 3). Cl/K ratios for all glasses are relatively low (0·03–0·04), indicating that assimilation of hydrothermally altered material did not occur during shallow-level crystallization. H_2O/Ce for the enriched glasses (Units 2 and 3) is significantly lower than Pacific and South Atlantic MORB values, suggesting that low H_2O/Ce is an inherent characteristic of the Kerguelen plume source. Vapor saturation pressures calculated using the H_2O and CO_2 contents of the glasses indicate that $\sim$1700 m of subsidence has occurred on this part of the plateau since eruption of the basalts at 34 Ma. Subsidence estimates for Site 1140 and other ODP drill sites indicate that the various parts of the Kerguelen Plateau subsided at a rate comparable with that for normal Indian Ocean lithosphere. Sulfur release to the Earth's atmosphere from 120 to 95 Ma, when the Southern and Central Kerguelen Plateau were constructed, could have had global climatic effects if the high latitude (low tropopause altitude) of the Kerguelen Plateau enabled powerful lava fountains to create convecting plumes that reached the stratosphere.

ACKNOWLEDGEMENTS

I would like to thank R. Guillemette and N. Shimizu for analytical assistance, Huai-Jen Yang for performing phase equilibrium calculations, D. Graham for providing me with the M.S. thesis of L. Douglas Priebe, and D. Clague, J. Dixon, and F. Frey for their helpful reviews of the manuscript. Funding was provided by the US Science Support Program (USSSP). The Ocean Drilling Program is sponsored by the National Science Foundation and participating countries under management of Joint Oceanographic Institutions, Inc. Secondary ion mass spectrometry analyses were performed at Woods Hole Oceanographic Institution in the Northeast National Ion Microprobe Facility, which was supported by grant EAR-9628749 from the National Science Foundation.

REFERENCES

Andres, R. J. & Kasgnoc, A. D. (1998). A time-averaged inventory of subaerial volcanic sulfur emissions. *Journal of Geophysical Research* **103**, 25251–25261.

Ariskin, A. A., Frenka, M. Y., Barmina, G. S. & Nielsen, R. L. (1993). COGMAGMAT: a FORTRAN program to model magma differentiation processes. *Computers and Geosciences* **19**, 1155–1170.

Batiza, R. & Vanko, D. (1984). Petrology of young Pacific seamounts. *Journal of Geophysical Research* **89**, 11235–11260.

Bonatti, E. (1990). Not so hot 'hotspots' in the oceanic mantle. *Science* **250**, 107–111.

Coffin, M. F. (1992). Subsidence of the Kerguelen Plateau: the Atlantic concept. In: Wise, S. W., Schlich, R., *et al.* (eds) *Proceedings of the Ocean Drilling Program, Scientific Results*, 120. College Station, TX: Ocean Drilling Program, pp. 945–949.

Coffin, M. F., Frey, F. A., Wallace, P. J., *et al.* (2000). Kerguelen Plateau–Broken Ridge: a large igneous province. *Proceedings of the Ocean Drilling Program, Initial Reports*, 183. College Station, TX: Ocean Drilling Program.

Coffin, M. F., Pringle, M. S., Duncan, R. A., Gladczenko, T. P., Storey, M., Müller, R. D. & Gahagan, L. A. (2002). Kerguelen hotspot magma output since 130 Ma. *Journal of Petrology* **43**, 1121–1139.

Crough, S. T. (1983). The correction for sediment loading on the seafloor. *Journal of Geophysical Research* **88**, 6449–6454.

Detrick, R. S., Sclater, J. G. & Theide, J. (1977). The subsidence of aseismic ridges. *Earth and Planetary Science Letters* **34**, 185–196.

Dixon, J. E. & Clague, D. A. (2001). Volatiles in basaltic glasses from Loihi seamount, Hawaii: evidence for a relatively dry plume component. *Journal of Petrology* **42**, 627–654.

Dixon, J. E. & Pan, V. (1995). Determination of molar absorptivity of dissolved carbonate in basanitic glass. *American Mineralogist* **80**, 1339–1342.

Dixon, J. E. & Stolper, E. M. (1995). An experimental study of water and carbon dioxide solubilities in mid-ocean ridge basaltic liquids. Part II: Applications to degassing. *Journal of Petrology* **36**, 1633–1646.

Dixon, J. E., Clague, D. A. & Stolper, E. M. (1991). Degassing history of water, sulfur, and carbon in submarine lavas from Kilauea volcano, Hawaii. *Journal of Geology* **99**, 371–394.

Dixon, J. E., Stolper, E. M. & Holloway, J. R. (1995). An experimental study of water and carbon dioxide solubilities in mid-ocean ridge basaltic liquids. Part I: calibration and solubility models. *Journal of Petrology* **36**, 1607–1631.

Dosso, L., Bougault, H., Beuzart, P., Calvez, J.-Y. & Joron, J. L. (1988). The geochemical structure of the South-East Indian Ridge. *Earth and Planetary Science Letters* **88**, 47–49.

Douglas Priebe, L. M. (1998). Geochemical and petrogenetic effects of the interaction of the Southeast Indian Ridge and the Amsterdam–Saint Paul Hotspot. M.S. thesis, Oregon State University, 232 pp.

Duncan, R. A. (2002). A time frame for construction of the Kerguelen Plateau and Broken Ridge. *Journal of Petrology* **43**, 1109–1119.

Duncan, R. A. & Storey, M. (1992). The life cycle of Indian Ocean hotspots. In: Duncan, R. A., Rea, D. K., Kidd, R. B., von Rad, U. & Weissel, J. K. (eds) *Synthesis of Results from Scientific Drilling in the*

Indian Ocean. Geophysical Monograph, American Geophysical Union **70**, 91–103.

Fine, G. & Stolper, E. (1986). Carbon dioxide in basaltic glasses: concentrations and speciation. *Earth and Planetary Science Letters* **76**, 263–278.

Fisk, M. R., Giovannoni, S. J. & Thorseth, I. H. (1998). Alteration of oceanic volcanic glass: textural evidence of microbial activity. *Science* **281**, 978–980.

Frey, F. A., Weis, D., Yang, H.-J., Nicolaysen, K., Leyrit, H. & Giret, A. (2000). Temporal geochemical trends in Kerguelen Archipelago basalts: evidence for decreasing magma supply from the Kerguelen plume. *Earth and Planetary Science Letters* **164**, 61–80.

Hayes, D. E. (1988). Age–depth relationships and depth anomalies in the Southeast Indian Ocean and South Atlantic Ocean. *Journal of Geophysical Research* **93**, 2937–2954.

Hofmann, A. W. (1997). Mantle geochemistry: the message from oceanic volcanism. *Nature* **385**, 219–229.

Ito, G. & Clift, P. D. (1998). Subsidence and growth of Pacific Cretaceous plateaus. *Earth and Planetary Science Letters* **161**, 85–100.

Kent, A. J. R., Clague, D. A., Honda, M., Stolper, E. M., Hutcheon, I. D. & Norman, M. D. (1999*a*). Widespread assimilation of a seawater-derived component at Loihi Seamount, Hawaii. *Geochimica et Cosmochimica Acta* **63**, 2749–2761.

Kent, A. J. R., Norman, M. D., Hutcheon, I. D. & Stolper, E. M. (1999*b*). Assimilation of seawater-derived components in an oceanic volcano: evidence from matrix glasses and glass inclusions from Loihi seamount, Hawaii. *Chemical Geology* **156**, 299–319.

Michael, P. J. (1995). Regionally distinctive sources of depleted MORB: evidence from trace elements and H_2O. *Earth and Planetary Science Letters* **131**, 301–320.

Michael, P. J. (1999). Implications for magmatic processes at Ontong Java Plateau from volatile and major element contents of Cretaceous basalt glasses. *Geochemistry, Geophysics, Geosystems*, **1,** 1999GC000025.

Michael, P. J. & Cornell, W. C. (1998). Influence of spreading rate and magma supply on crystallization and assimilation beneath mid-ocean ridges: evidence from chlorine and major element chemistry of mid-ocean ridge basalts. *Journal of Geophysical Research* **103**, 18325–18356.

Moore, J. G. (1970). Water content of basalt erupted on the ocean floor. *Contributions to Mineralogy and Petrology* **28**, 272–279.

Nakamoto, K. (1978). *Infrared and Raman Spectra of Inorganic and Coordination Compounds*, 3rd edn. New York: John Wiley, 448 pp.

Nicolaysen, K., Frey, F. A., Hodges, K., Weis, D. & Giret, A. (2000). $^{40}Ar/^{39}Ar$ geochronology of flood basalts, from the Kerguelen Archipelago, southern Indian Ocean: implications for Cenozoic eruptive rates of the Kerguelen Plume. *Earth and Planetary Science Letters* **174**, 313–328.

Pringle, M. S. & Duncan, R. A. (2000). Basement ages from the Southern and Central Kerguelen Plateau: initial products of the Kerguelen Large Igneous Province. *EOS Transactions, American Geophysical Union* **81**, 424.

Pringle, M. S., Storey, M. & Wijbrans, J. (1994). $^{40}Ar/^{39}Ar$ geochronology of mid-Cretaceous Indian Ocean basalts: constraints on the origin of large flood basalt. *EOS Transactions, American Geophysical Union* **75**, 728.

Pyle, D. M., Beattie, P. D. & Bluth, G. J. S. (1996). Sulphur emissions to the stratosphere from explosive volcanic eruptions. *Bulletin of Volcanology* **57**, 663–671.

Royer, J.-Y. & Coffin, M. F. (1992). Jurassic to Eocene plate tectonic reconstructions in the Kerguelen Plateau region. In: Wise, W. S., Schlich, R., *et al.* (eds) *Proceedings of the Ocean Drilling Program, Scientific Results*, 120. College Station, TX: Ocean Drilling Program, pp. 917–928.

Royer, J.-Y. & Sandwell, D. T. (1989). Evolution of the Eastern Indian Ocean since the late Cretaceous: constraints from Geosat altimetry. *Journal of Geophysical Research* **94**, 13755–13782.

Schilling, J. G., Bergeron, M. B. & Evans, R. (1980). Halogens in the mantle beneath the North Atlantic. *Philosophical Transactions of the Royal Society of London, Series A* **297**, 147–178.

Self, S., Keszthelyi, L. & Thordarson, Th. (1998). The importance of pahoehoe. *Annual Review of Earth and Planetary Sciences* **26**, 81–110.

Shimizu, N. (1998). The geochemistry of olivine-hosted melt inclusions in a FAMOUS basalt ALV519-4-1. *Physics of the Earth and Planetary Interiors* **107**, 183–201.

Shimizu, N. & Hart, S. R. (1982). Applications of the ion microprobe to geochemistry and cosmochemistry. *Annual Review of Earth and Planetary Sciences* **10**, 483–526.

Stothers, R. B., Wolff, J. A., Self, S. & Rampino, M. R. (1986). Basaltic fissure eruptions, plume heights, and atmospheric aerosols. *Geophysical Research Letters* **13**, 725–728.

Sun, S. S. & McDonough, W. F. (1989). Chemical and isotopic systematics of oceanic basalts: implications for mantle composition and processes. In: Saunders, A. D. & Norry, M. J. (eds) *Magmatism in the Ocean Basins. Geological Society, London, Special Publications* **42**, 313–345.

Wallace, P. & Carmichael, I. S. E. (1992). Sulfur in basaltic magmas. *Geochimica et Cosmochimica Acta* **56**, 1863–1874.

Wallace, P. J. & Carmichael, I. S. E. (1994). Sulfur speciation in submarine basaltic glasses as determined by measurements of S*Kα* X-ray wavelength shifts. *American Mineralogist* **79**, 161–167.

Weis, D. & Frey, F. A. (2002). Submarine basalts of the Northern Kerguelen Plateau: interaction between the Kerguelen plume and the Southeast Indian Ridge revealed at ODP Site 1140. *Journal of Petrology* **43**, 1287–1309.

Weis, D., White, W. M., Frey, F. A., Duncan, R. A., Dehn, J., Fisk, M., Ludden, J., Saunders, A. & Storey, M. (1992). The influence of mantle plumes in generation of Indian oceanic crust. In: Duncan, R. A., Rea, D. K., Kidd, R. B., von Rad, U. & Weissel, J. K. (eds) *Synthesis of Results from Scientific Drilling in the Indian Ocean. Geophysical Monograph, American Geophysical Union* **70**, 57–89.

Weis, D., Frey, F. A., Leyrit, H. & Gautier, I. (1993). Kerguelen Archipelago revisited: geochemical and isotopic study of the Southeast Province lavas. *Earth and Planetary Science Letters* **118**, 101–119.

Yang, H.-J., Kinzler, R. J. & Grove, T. L. (1996). Experiments and models of anhydrous, basaltic olivine–plagioclase–augite saturated melts from 0·001 to 10 kbar. *Contributions to Mineralogy and Petrology* **124**, 1–18.

Yang, H.-J., Frey, F. A., Weis, D., Diret, A., Pyle, D. & Michon, G. (1998). Petrogenesis of the flood basalts forming the Northern Kerguelen Archipelago: implications for the Kerguelen Plume. *Journal of Petrology* **39**, 711–748.